Chapter 2

The 3D radiative hydrodynamic model

Contents

2.1 Model atmospheres : from one-dimensional to three-dimensional models 11

2.2 The 3D radiative hydrodynamic model CO^{5}BOLD 13

2.2.1 Model computation 14

2.3 Modelling RSG stars 22

2.3.1 Surface pattern and convective structure 23

2.3.2 Model structure 27

2.3.3 Waves and shocks 28

2.3.4 Computational time 29

2.1 Model atmospheres : from one-dimensional to three-dimensional models

One-dimensional representations of stellar surface layers and envelopes have traditionally been the only option available. Unfortunately, a rigorous theory of stellar convection is lacking due to the complexity of the hydrodynamical problem. So far, stellar structure models rely on a simply approach called *Mixing − length theory* (MLT), or other variants. The properties of convection are estimates from either local or non-local formulae and all the quantities are one-dimensional (i.e. they depend on the radius).
Alternatively, radiation hydrodynamics simulations can provide physically consistent *ab initio* models of stellar convection.
1D models are in many cases static and local. As a result, it is necessary to calibrate the resulting models, using parameters either built into the description from the start, or parameters introduced specifically for the purpose of calibration. Nevertheless, the relative simplicity of treatment and the associated low computational cost are the main advantages of one-dimensional (1D) approach.

Three-dimensional (3D) models are much more computer intensive but they have advantages of being *ab initio*, time-dependent, multi-dimensional and non-local. The principal differences between one-dimensional and three-dimensional models are reported in Tab. 2.1.

Table 2.1: One-dimensional versus three-dimensional models

One-dimesional models	Three-dimensional models
(+) Detailed radiative transfer	(-) Radiative transfer
	grey or opacity binning (5 bins)
(-) Time-independent	(+) Time-dependent
(-) No temperature inhomogenity	
(+) Relative simplicity of treatment	(+) Radiation and hydrodynamics coupled
(-) Free Parameters	(-) Free parameters (boundary conditions,
(MLT, micro and macro turbulence)	numerical resolution, viscosity tensor, time-step control)
(-) Convection (Mixing Length Theory)	(+) Proper treatment of convection *ab initio*
(-) Radiative Equilibrium	
(-) (Usually) LTE	(-) LTE
(+) CPU-friendly	(-) CPU-demanding

3D models are necessary for a proper, qualitative and quantitative analysis of the surface of most stars, in order to have parameter-free estimation of the convection. Furthermore, 3D models represent a reliable way to utilize the abundance of information that is encoded in the detailed shapes of photospheric spectral lines (this is true for 3D local solar models but still not validated for the global simulations of RSG).
Three-dimensional radiative hydrodynamics simulations are no longer restricted to the Sun but cover a substantial portion of the Hertzsprung-Russell diagram (see Fig. 2.1). Those who have been very successful as a tool to understand solar granulation by modeling small patches of the surface are Nordlund (1982), Steffen et al. (1989), Asplund et al. (2000a), Skartlien et al. (2000), Stein & Nordlund (2000), Gadun et al. (2000), Robinson et al. (2003), Vögler (2004). Freytag et al. (1996) extended these simulations to other main-sequence stars, Ludwig et al. (1994) and Freytag et al. (1996) to white dwarfs, and Freytag & Salaris (1999) to subgiants. The simulations of red giants by Asida & Tuchman (1997) (see also Asida 2000 2003) use the 2D VULCAN code with non-carthesian grid, and cover a substantial fraction of the stellar surface. Red giant stars have been simulated also by Collet et al. (2007) using the radiation hydrodynamics code by Stein & Nordlund (1998).
RSG stars have been simulated for the first time by F2002, the continuation of this work led to higher-spatial resolution models (particularly important for the surface layers) and can be found in a paper by Freytag (2008, in preparation and Sect. 2.3).
Furthermore, RHD models have been used to determine the solar abundances by Asplund et al. (2004) using the Nordlund-Stein code. Independent redetermination of these abundances with CO^{5}BOLD simulations are in progress (Ludwig & Steffen 2007).

Concerning RSG stars, the low surface density implies that the convective velocities must necessarily become increasingly supersonic and conventional one-dimensional models may become particularly inaccurate in this regime because of the MLT approximation for estimating convective energy transport. In fact, the MLT assumption of pressure

equilibrium between a convecting element and its surrounding would fail because the time required for pressure equilibrium to become established in the element is larger than the lifetime of the element itself. Furthermore, since the size of the convection cells start to become comparable to the entire envelope, it is necessary to model the star as a whole with the 3D RHD simulation (see Sect. 2.3).

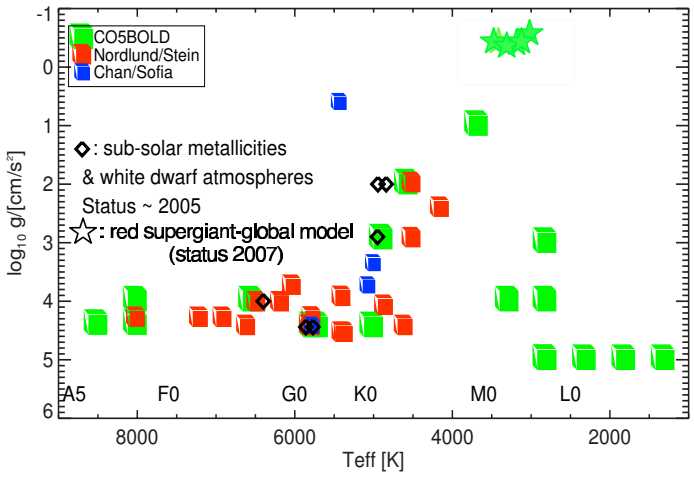

Figure 2.1: Distribution in the Hertzsprung-Russell diagram of realistic 3D stellar convection models computed by different group (Figure adapted from Steffen 2006). Convection simulations are no longer restricted to the Sun.

2.2 The 3D radiative hydrodynamic model CO^{5}BOLD

Radiative transfer in three-dimensional models is still a hard task to achieve. The actual limitation for these simulations is the CPU-time. The radiative transfer is treated at the strict LTE and a frequency independent or non-grey opacity treatment (with five wavelength groups) is employed. Still, This treatment is far from the detailed radiative transfer calculation done in one-dimensional models.
CO^{5}BOLD (COnservative COde for the COmputation of COmpressible COnvection in a BOx of L Dimensions, L=2,3") is developed by B. Freytag, M. Steffen and H-G Ludwig, and collaborators (F2002). It is used for modeling solar and stellar surface convection. The time-dependent hydrodynamics equations coupled with the radiative transfer equation are solved for a fully compressible, chemically homogeneous plasma in a gravitational field in two or three spatial dimension.
It uses operator splitting to separate the various (explicit) operators: the hydrodynamics, the tensor viscosity, the radiation transport. The hydrodynamics module is based on a finite volume approach and relies on operator (directional) splitting to reduce the 2D or 3D problem to one dimension, where a 1D Riemann solver (Roe-type, Roe 1986) is applied, modified to account for a realistic equation of state, a non-equidistant Cartesian grid, and the presence of source terms due to an external gravity field. The equation of state is not computed at the run time but has been tabulated in advance to save computational

time. It takes into account, for any prescribed chemical composition, HI, HII, H_2, HeI, HeII, HeIII and a representative metal. The release of ionization energy (latent heat) is an important factor that influences the onset and strength of stellar convection.
Two different geometry can be used with CO^{5}BOLD: the STAR-IN-A-BOX setup that is used to model red supergiant stars, and the BOX-IN-A-STAR setup used to model a statistically representative volume of the stellar atmosphere.
CO^{5}BOLD can run on a variety of different hardware architectures, from simple desktop computers to multi-processor clusters on which the parallelisation via OpenMP is implemented. Furthermore, CO^{5}BOLD has a modular structure which maintains a remarkable flexibility. Some more technical information are available on the online manual[5] and in a paper by Freytag (F2002).
In the next Sections, I will follow the principal steps of the model computation showing the principal characteristics of the global and local models.

2.2.1 Model computation

As input parameters, CO^{5}BOLD needs the surface gravity and the specific entropy of the material entering in the computational volume from the lower open boundary (box-in-a-star setup) or from the center of the box (star-in-a-box setup). The entropy strongly affects the amount of heat entering the computational volume. In the case or RSG, inside a sphere of radius r_0, the internal energy is adjusted to keep the entropy production close to some desired value. This replaces the energy production by nuclear fusion in the real stellar core (see F2002).
Two important files are necessary at the beginning of the simulation, the parameter file and the star file. The first file includes all relevant numerical parameters, that define the hydrodynamical scheme, the viscosity[6], radiative transfer (e.g., the number of frequency bins if it is possible to switch to non-grey), the boundary conditions, the desired time increment for the output data, and the length of the simulation. The second file can be an ad-hoc starting model created for the desired stellar atmosphere, or a final state of a preceding model which can be modified as required. Moreover, information about equation of state and opacity table to be used are present in the parameter file.
The operator splitting reduces the calculation to several independent steps (Fig. 2.2). For each time step, the hydrodynamics is treated first, resulting in updates of the basic set of quantities in all grid cells. These quantities are updated again after the radiation transfer step for this time step.

[5] www.astro.uu.se/~bf/co5bold_main.html

[6] The hydrodynamics scheme is stable enough to handle one-dimensional and most multi-dimensional problems. However, there are special multi-dimensional cases that make an additional tensor viscosity necessary to ensure stability. In a separate sub step, see Fig. 2.2, CO^{5}BOLD viscous energy fluxes are computed and used to update the velocities and the internal energy. The turbulent eddy viscosity is of Smagorinsky (1963) type and a typical turbulent Prandtl number is 6 for RSGs.

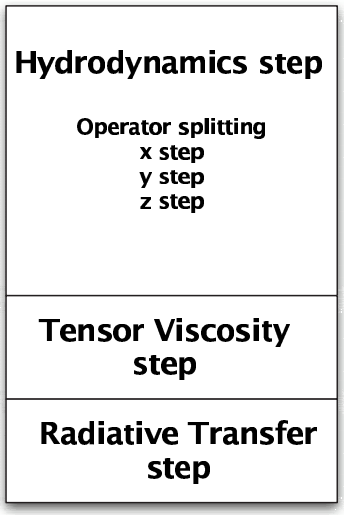

Figure 2.2: Single timestep in CO5BOLD. The operator splitting divides the step into independent steps.

Hydrodynamic equations

The hydrodynamics equations solved by CO5BOLD are

$$\frac{\partial \rho}{\partial \mathrm{t}} = -\nabla \left(\rho \vec{\mathrm{v}}\right) \tag{2.1}$$

$$\frac{\partial \rho \vec{\mathrm{v}}}{\partial \mathrm{t}} = -\rho \left(\vec{\mathrm{v}} \cdot \nabla\right) \vec{\mathrm{v}} - \nabla P - \rho \vec{\nabla} \Phi \tag{2.2}$$

$$\frac{\partial \rho \epsilon_{ik}}{\partial \mathrm{t}} = -\nabla \cdot \left[\left(\rho \epsilon_{ik} + \mathrm{P}\right) \vec{\mathrm{v}}\right] - \rho \vec{v} \cdot \left(\vec{\nabla} \Phi\right) + \mathrm{Q}_{\mathrm{rad}} \tag{2.3}$$

where ρ is the density, $\vec{\mathrm{v}}$ is the velocity, P is the total pressure (the radiative pressure is not included in the models presented in this work), $\vec{\nabla}\Phi = \vec{\mathrm{g}}$ is the gravitational force, $\mathrm{Q}_{\mathrm{rad}}$ is the radiative heating rates (see Eq. 2.5) and ϵ_{ik} is the total energy density (i.e., the specific internal energy plus the kinetic energy).
The first equation represents the continuity equation, the second is the Eulerian equation of motion, and the third energy equation. They represent the conservation of mass, momentum, and energy respectively.

Computational domain

The numerical grid is of Cartesian geometry and it can be two or three dimensional. The grid is fixed in time but it can be non-equidistant (box-in-a-star setup) or equidistant (star-in-a-box setup). All the quantities that result from the simulation, are stored at the center of the cell. Next to the centers of the cells, also the boundary are provided (this is important for hydrodynamics step). In the case of the star-in-a-box setup, the computational domain is a cube with an equidistant grid in all direction. All six surfaces of the computational box employ the same open boundary conditions. The box-in-a-star

setup has periodic lateral boundaries, while the bottom and top boundaries are open and transmitting.

Local and global models

The local models work with the BOX-IN-A-STAR setup and they are suitable, e.g., for solar-type granulation. The spatial scale of the solar granulation ($x_{gran} \approx 2000$km) is much smaller than the solar radius ($R_\odot \approx 700000$km). It is then impossible to model the whole solar convection zone in a single simulation which at the same time has to account for the global large-scale flows and small-scale surface structures. In local models, only a small portion of the uppermost layers of the convection zone is simulated. Fig. 2.3 shows examples of local boxes for different stars. These models enclose the transition between the optically thick layer and the optically thin photosphere, where the ascending plasma from the interior looses its energy by efficient radiative cooling.

The global models use the STAR-IN-A-BOX setup (Fig. 2.4). This configuration is used to simulate the whole star and is the setup of choice to simulate the RSGs. As already mentioned in previous sections, all six surfaces of the computational box employ the same open boundary conditions. In addition there is an inner boundary condition: within a radius r_0, the gravitational potential is smoothed (see Eq. 2.4) and in this sphere a source term to the internal energy provides the stellar luminosity. The hydrodynamics and the radiative transfer scheme ignore it and integrate through the model core.

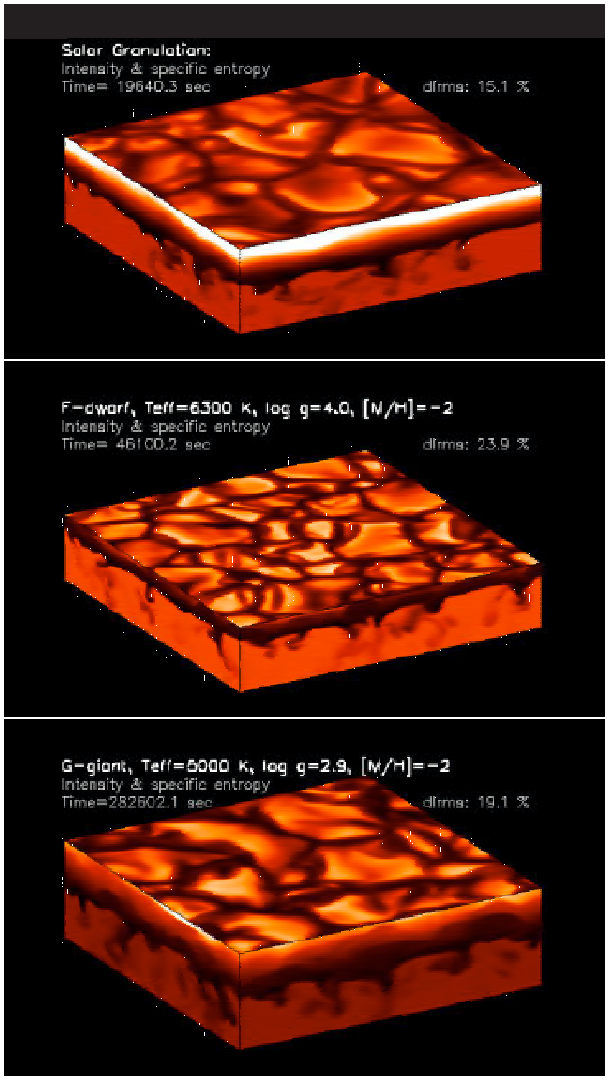

Figure 2.3: Snapshots from 3D local models showing the emergent intensity at $\lambda = 6200$Å (top face), and the specific entropy (sides) for the solar granulation (T_{eff}=5770K, log$g$= 4.44, solar metallicity, dimension of the box 5.6x5.6x2.25 Mm, *top*), a metal-poor F dwarf (T_{eff} = 6300K, log$g$= 4.0, [M/H]=-2, dimension of the box 28.6x28.6x7 Mm, *middle*), and a metal-poor G giant (T_{eff}=5000K, log$g$= 2.9, [M/H]=-2, dimension of the box 126x126x47 Mm, *bottom*). Figure from F2002.

Gravitational potential

In the case of the box-in-a-star setup, the gravitation is constant. This is legitimate in view of the limited height extend of the computational box and the corresponding small change of the gravitational potential.
For the star-in-a-box setup, the acceleration due to gravity is derived from a spherical potential

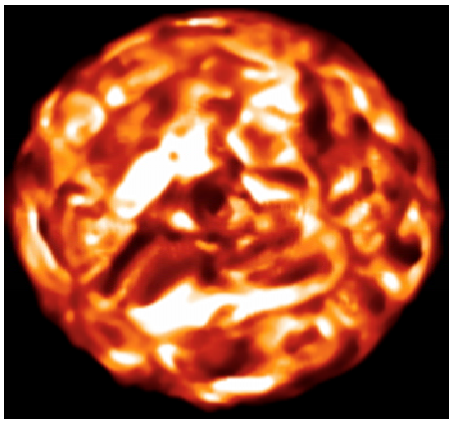

Figure 2.4: Grey surface intensity for a snapshot from a three-dimensional global simulation of the red supergiant simulations st35gm03n07 in Tab. 4.1. T_{eff}=3495.2±14.3 K, log$g$= -0.35, [M/H]=0, dimension 126x126x47 Mm, the dimensions of the box are 2081x2081x2081 $R_\odot$.

$$\Phi = -\frac{GM_*}{\left(r_0^4 + r^4/\sqrt{1+(r/r_1)^8}\right)^{1/4}} \tag{2.4}$$

where M_* is the mass of the star to be modeled and r_0 and r_1 are free smoothing parameters. The r_0 and r_1 are the inner and outer smoothing radius and they are used to flatter the potential further out. This lowers gravity and increases the scale height. Without that, the density can drop too steeply. These parameters are set by hand, so that the density does not drop too much, while not affecting the photospheric layers too strongly. In some models it is set to large values (beyond the extension of the box). As long as $r_0^4 << r^4 << r_1^4$, $\Phi = -\frac{GM_*}{r}$. For $r \to 0$, $\Phi = -\frac{GM_*}{r_0}$ and for $r \to \infty$, $\Phi = -\frac{GM_*}{r_1}$. Typically, the inner smooth radius is 0.2 stellar radii and the outer smooth radius is set outside the box (see F2002 for details).

Radiative transfer methods

The iteration between radiation and gas plays an important role in the hydrodynamics of stellar atmosphere. The net amount of heat per unit mass and time, q, transferred between the radiation field and matter is given by

$$q = \frac{Q_{rad}}{\rho} = 4\pi \int_0^\infty \chi_\nu \left(J_\nu - S_\nu\right) d\nu \tag{2.5}$$

where χ_ν is the absorption coefficient per unit mass including scattering term, S_ν the source function, and J_ν the angular average intensity. The strict Local Thermal Equilibrium is assumed with the source function equal to the Planck function.

CO5BOLD's users have the choice, for solving the non-local equation of radiative transfer, to use *long characteristic method*, developed by M. Steffen and used in the box-in-a-star setup, and the *short characteristic method* developed by B. Freytag and used in the star-in-a-box setup. In this thesis both methods are used to compute local and global models (see Fig. 2.5).
The short characteristic method follows the radiation through a single cell at a time. To account for the short radiative time-scale, several (typically 6 to 9) radiative sub-steps are performed per global step. Each sub-step uses only 3 rays (e.g. in the directions $(1,1,0)$,$(1,-1,0)$,$(0,0,1)$ or $(1,0,1)$,$(1,0,-1)$,$(0,1,0)$ or $(0,1,1)$,$(0,1,-1)$,$(1,0,0)$) or 4 rays (along the space diagonals $(1,\pm1,\pm1)$). These sub-steps are performed cyclically in order to compute all 13 ray directions within a global time step.

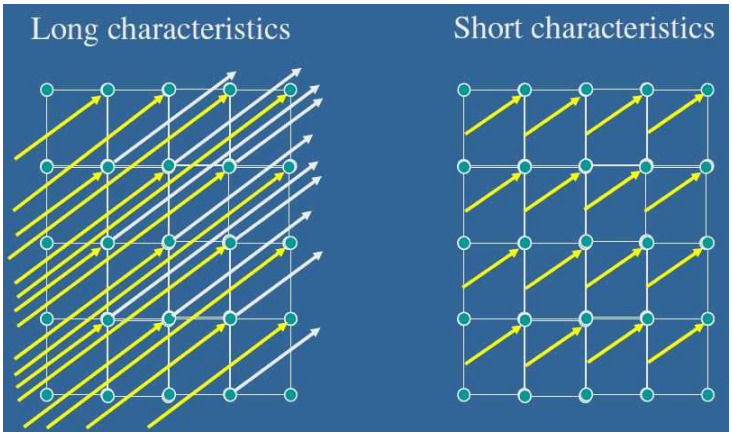

Figure 2.5: Long and Short characteristic methods for solving radiation transfer equation.

In case of long characteristics, the non-local equation of radiative transfer is solved along a large number of rays that traverse the computational box under various azimuthal and inclination angles (typically 6 polar and 4 azimuthal angles). The spatial resolution obtained by the rays can be finer than the one of the hydrodynamics grid. This is important in the presence of a large variation of the radiation field in the vicinity of a shock wave. Along the ray, the one-dimensional radiative transfer is solved applying the Feautrier (Feautrier 1964) method (see Mihalas, 1978).
The solution finally results in the radiative fluxes and heating rate Q_{rad} (see Eq. 2.3). For every time-step the radiation field has to be computed several times to achieve the accuracy searched. Eventually, Q_{rad} is interpolated back into the hydrodynamics grid. This important rate represents the change in internal energy due to radiation transport. The periodic boundaries imply that each ray is continued across the boundary and re-enters on the other side of the box.

Mean absorption coefficients

The definition of the mean absorption coefficients are necessary for the next Sect. about the grey and non-grey radiative transfer.
Frequency independent opacity means can be done with several methods :

- Rosseland mean absorption coefficient. This is an harmonic mean, i.e. the average of a reciprocal quantity, which favors frequencies with the smallest opacities.

$$\frac{1}{\bar{\mathrm{k}}_{\mathrm{Ross}}} = \frac{\int \frac{1}{\mathrm{k}_\nu} \frac{d\mathrm{B}_\nu}{d\mathrm{T}} d\nu}{\int \frac{d\mathrm{B}_\nu}{d\mathrm{T}} d\nu} \tag{2.6}$$

- Planck mean absorption coefficient. This is a linear mean.

$$\bar{\mathrm{k}}_{\mathrm{Planck}} = \frac{\int \mathrm{k}_\nu \mathrm{B}_\nu \mathrm{d}\nu}{\int \mathrm{B}_\nu \mathrm{d}\nu} \tag{2.7}$$

The Plank mean opacity is constructed to yield the correct integrated value of the thermal emitted radiation represented by the Planck function. Planck mean becomes consistent with the requirement of the radiation equilibrium only near the surface where the material becomes optically thin at all frequencies. It leads to inaccuracies in the deduced model atmosphere structure and in the predicted emerging spectrum because only emission as source of radiation is considered. The light is blocked excessively due to over-emphasizing of strong spectral lines. As a consequence, the underlying layers are heated by the energy hindered from escaping.
The harmonic nature of the averaging process for the Rosseland mean gives higher weight to frequency regions with low opacities where therefore the greatest amount of radiation will be transported. The effect of continuum points is over-emphasized. The energy will escape too easily and the stellar atmosphere geometrically contracts. The Rosseland mean leads a poor approximation to the energy balance near the surface and underestimates the opacity there. It is valid only at great optical depth. The use of the Rosseland mean is consistent with the diffusion approximation[7] of the transfer equation.

Opacity tables

The frequency dependance of the radiation field can be represented by two approaches: either the *grey* approximation, that completely ignores the frequency dependence, and the more elaborate scheme accounting for *non-grey* effects which is based on the idea of "opacity binning" (Nordlund 1982; Nordlund & Dravins 1990). The basic approximation is the so called *multi-group scheme* (Ludwig 1992 and Ludwig et al. 1994).
In the *grey approximation*, where the whole relevant range is binned into one frequency set, the Rosseland mean opacities are calculated. In the *multi-group scheme*, the opacity groups for the non-grey case are obtained by sorting the mean absorption coefficients at different frequencies as follows: a one-dimensional model atmosphere is assumed to calculate a monochromatic optical depth scale τ_ν for each frequency separately.
The geometrical height where $\tau_\nu = 1$ is thus dependent on frequency. The optical depths τ_{Ross} is calculated for the frequency-independent Rosseland mean, and a set of intervals

[7] Diffusion approximations is valid at depths in the medium much larger than a photon mean-free-path, the radiation is trapped, becomes essentially isotropic, eventually approaches thermal equilibrium (S_ν=B_ν). Diffusion approximation can be used as a lower boundary conditions on the transfer equation in a semi-infinite atmosphere.

($\tau_{\rm Ross}^{i-1} \geq \tau_{\rm Ross}\,(\tau\nu = 1) > \tau_{\rm Ross}^{i}$) is defined. For every frequency set, *Planck* and/or *Rosseland* means or a hybrid form are calculated for a pre-set chemical composition and thermal state of the gas. Then, the monochromatic coefficients are sorted into the appropriate group by their corresponding position $\tau_{\rm Ross}\,(\tau_\nu = 1)$ on the Rosseland scale. For every frequency set, the opacity is given by the Planck mean in the optically thin layers and by the Rosseland mean in the optically thick layers (see Ludwig et al. 1994) for details).
In the box-in-a-star setup the grey or the non-grey treatment can be chosen. In the star-in-a-box setup, we have use almost exclusively the grey approximation and the opacity table has been merged at around $12000K$ from high temperature OPAL data (Iglesias et al. 1992) and low temperature PHOENIX data (Hauschildt et al. 1997) by H-G Ludwig. For the non-grey, five wavelength groups are employed to describe the wavelength dependence of the radiation field. The group averaged opacity are based on data from MARCS code (Gustafsson et al. 1975, Plez et al. 1992 and Gustafsson et al. 2008).
An exploratory model computed with five wavelength groups based on MARCS opacities is discussed in Chapter 9.

Equation of State

The equation of state characterizes the thermodynamic state of matter. In the case of an ideal gas, it can be written as

$$\mathrm{P} = \frac{\mathrm{R}}{\mu}\rho\mathrm{T} \tag{2.8}$$

where three thermodynamic variables (pressure, P, density, ρ, temperature, T) are linked. R= $8.31 \times 10^7 \mathrm{ergK^{-1}g^{-1}}$ and is the universal gas constant, and μ is the dimensionless mean molecular weight.
In stars, a proper treatment of this equation must take into account the ionization of atoms, as well as the dissociation and recombination of molecules. The solution of the Saha equation, molecules, and conservation relations for charge and mass are required. The resulting values are pre-tabulated and used if CO5BOLD.

Output data

3D simulations result into a large amount of data. The architecture data format used is called UIO (developed by B. Freytag, more details on the online CO5BOLD manual). The resulting files have the following extension :

- "full" file contains all the important variables at each grid point of the computational box
- "mean" file contains a large number of averaged variables in model slices
- "end" file contains the updated variables of the last timestep of the simulation
- "fine" file contains variables linked with M. Steffen radiative transfer module

For RSG simulations, the full file is written every $\approx$ 2000000s (about 21 days) and the mean file every $\approx$ 500000s.

Table 2.2: Characteristics of local and global models - Summary

Star-in-a-box setup	Box-in-a-star setup
spherical potential	gravitation is constant
cube with an equidistant grid in all directions,	periodic lateral boundaries,
same boundary condition for all six surface	open bottom and top boundaries
short-characteristics method	long-characteristics method
LTE	LTE
grey scheme	grey or non-grey scheme

2.3 Modelling RSG stars

The most important parameters that determine the type of the modeled star is the input luminosity into the core and the mass. The stellar mass enters in equation 2.4 for the gravitation potential. Our simulations have a solar chemical composition. There is no stellar structure model for RSG implemented, but CO^{5}BOLD integrates the stratification structure from outside and stops when the core is reached. The central temperature is over 300000 K. The effective temperature, the radius and the surface gravity are an outcome of the simulation that varies with time following changes in the granulation pattern (see Sect. 4.2 for the definition of these parameters).
Fig. 2.6 shows the grey intensity emerging on one side of the computational cube. The starting model is a sphere in hydrostatic equilibrium with a small velocity field coming from a previous relaxed model. A regular pattern of small-scale convection cells develops initially and then, as the cells merge, the average structure becomes big and the regularity is lost. The contrast grows. After about 5 years, the state is relaxed and the pattern becomes completely irregular. In the beginning, the entire surface becomes darker. This is due to the fact that there is a radiative energy loss with no convective supply from the interior, yet (see Sect. 2.3.2).

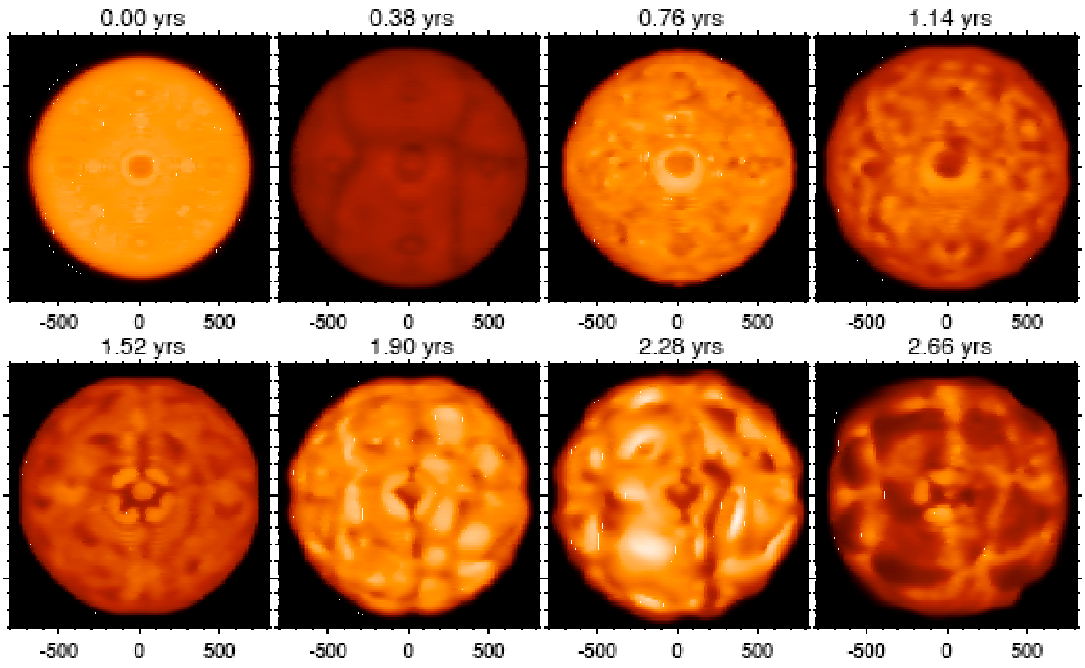

Figure 2.6: Initial sequence of a red supergiant star RHD simulation. Grey intensity with axes in solar radii (image courtesy of Bernd Freytag, 2008 in preparation).

2.3.1 Surface pattern and convective structure

The relaxed model snapshot in Fig. 2.4 shows that the surface is speckled with high contrast structures. Since the bolometric intensity is represented, the convective cells are hard to discern (see Chapter 8 for a detailed analysis of wavelength dependent intensity maps). In general, the surface of the supergiant model is covered by small convective cells with shirking plumes that end not too far below the surface. These elements with a lifetime of weeks or months live on the top of a few large envelope cells with lifetime of years and downdrafts that can penetrate down to the model core.
In Fig. 2.7, the temperature isosurfaces indicate that the large convective pattern is still visible at 20000, 30000 and 100000 K (i.e., stellar interior just below the surface, see Fig. 2.9). The downdrafts at the borders of the large envelope cells almost traverse the entire envelope and a deep large-scale network of intergranular lanes is formed. In all the density plots the atmospheric pressure waves are above the convection zone and hide it.

The overturning convective flow field in the interior and lower in the lower photosphere is separated from the shockwave dominated (red arrow in Fig. 2.8) outer atmosphere by a clear border (light blue, Fig. 2.8). The temperature is about 300000 K in the core, about 20000K just below the surface, and 1600-3500 K in the photosphere. The vorticity[8]

[8]The vorticity, $\vec{\omega}$ is the circulation per unit area at a point in a fluid flow field. It is a vector quantity, whose direction is along the axis of the fluid's rotation: $\vec{\omega} = \vec{\nabla} \times \vec{v}$

Figure 2.7: Temperature (top row) and density (bottom row) isosurfaces. The image has been made using the visualization program in Appendix F. The model and timestep is the same as in Fig. 2.8

component perpendicular to the image (Fig. 2.9) shows that there is a strong general infall of material. This picture changes over time.
The downdrafts oscillate back and forth and have changing in the vertical extent. Often the lower tip is cut off and disconnected cool bubbles travel inward until they mix with the surrounding material. While the individual vortices in the downdrafts have a very short lifetime, there is a strong and persistent downfall region that can live for years (the lifetime of the giant envelope cells). The convective turnover time for a full cycle (surface-center-surface) is long (few years). The lifetime of large cells is typically several turnover times. In longer simulations of smaller stars ($5M_{\odot}$ supergiant and $1M_{\odot}$ AGB stars) the global pattern change and the large granules broke up (B. Freytag private communication). However, the statistics is poor and a good value for the typical lifetime of the large cells cannot be given. Qualitatively, it is several years.

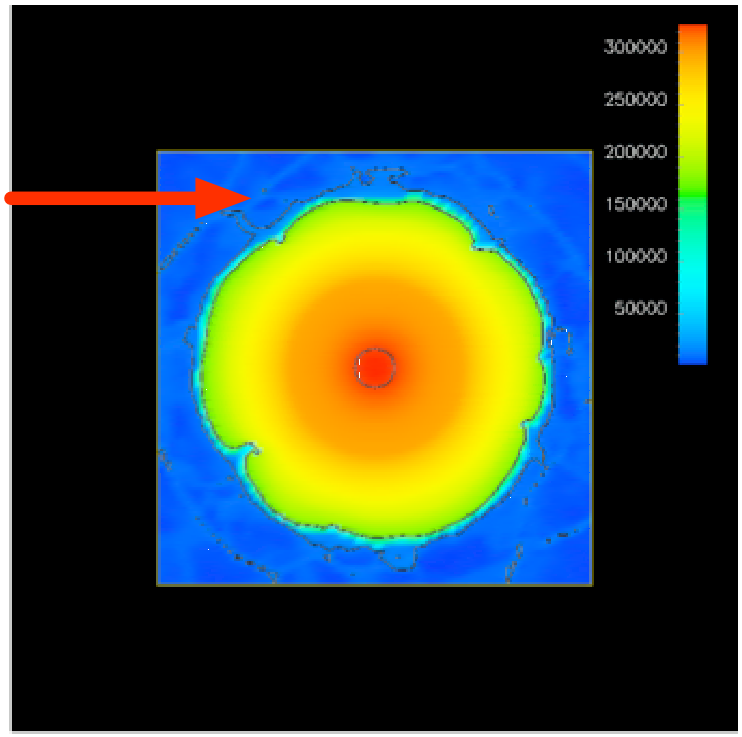

Figure 2.8: Temperature of a two-dimensional slice through the center of the model. The contour lines correspond to T=1600K, 3500K, 20000K, and 300000K (the image has been made using the visualization program in Appendix F).

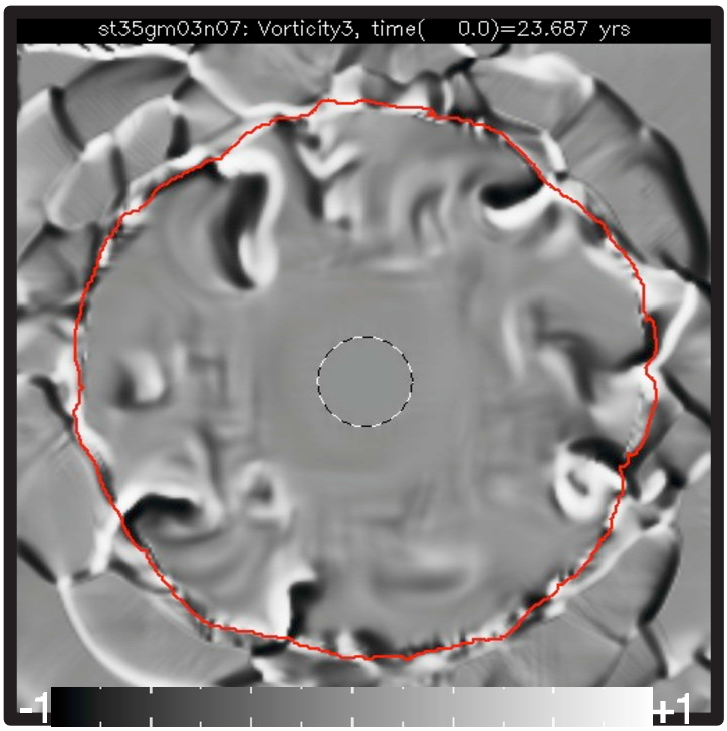

Figure 2.9: Vorticity component perpendicular to the image plan. The red line is the approximate position of the surface ($\tau_{Rosseland} = 1$) and the dashed line in the center denotes the stellar core. Black regions correspond to vorticity equal to -1 and bright region to vorticity equal to +1. Same slice as in Fig. 2.8

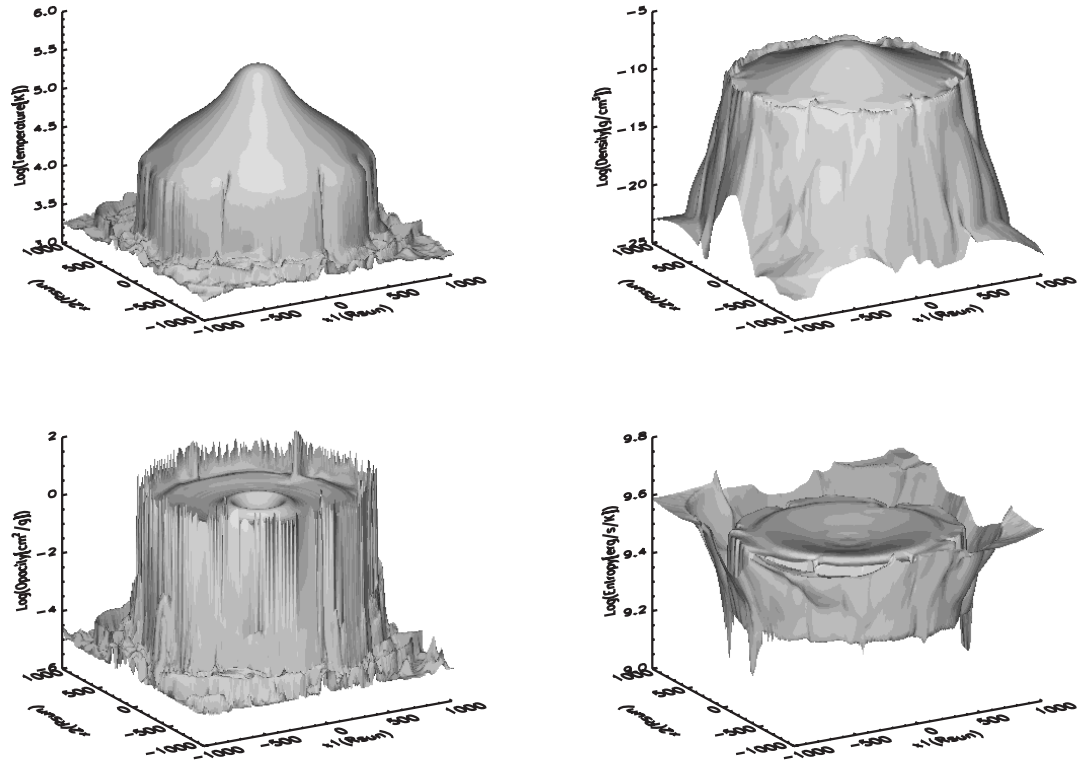

Figure 2.10: Logarithm of temperature, density, opacity and entropy of a slice through the center from a snapshot of a RSG simulation (st35gm03n07 in Tab. 4.1).

2.3.2 Model structure

The opacity peaks around T=13000 K just below the photosphere (Fig. 2.10, bottom left panel) and this causes the steep temperature jump (top left panel). As a consequence, there is a density inversion (top right panel). This inversion layer is a sign of convective instability.
The upper envelope of the entropy is almost totally flat (lower right panel) and the temperature gradient is close to adiabatic. Near the surface, the entropy gradient steepens and become extremely large, in what is called the superadiabatic region. The entropy drop occurs in a very thin layer. Its strong gradient cause a large buoyancy and renders the convective motions, in competition with the radiative energy transport, more violent.

2.3.3 Waves and shocks

Fig. 2.11 shows the local generation of sound waves in the interior, that propagate up to the envelope attending their final transformation into shocks in the photosphere. For example, a ring-like wave with a diameter of about 500 R$\odot$ is visible in the last frame; also the emitting region situated northeast of the center is obvious. The nonstationarity is a prerequisite for wave excitation, it is amplified by the surface granules fall into downdrafts. A wave train starts as small pressure fluctuation in the interior. Once the spherical waves arrive in the photosphere, they are shaped by the convective cells.
The sharp drop in temperature (Fig. 2.10, upper left panel) and sound speed at the surface leads to a compression of the wave train, and the increase of the density in the inversion layer (Fig. 2.10, upper right panel) leads to a decrease of the amplitude. Eventually, due to the small density scale height the wave amplitude increases again rapidly in the photosphere achieving velocities of the order of 10 to 20 km/s. Within the range of available grids (95^3 to 315^3) the qualitative behavior is the same.
The shocks can extend over large fractions of the surface. This is remarkable in Fig. 2.11 where there is a shock wave hovering just above the stellar surface (black arrow) because it has to move against the infalling material. Other shocks can originate closer to a point in the surface and remain localized to a certain region of the surface (Fig. 2.11, lower right corner of the panels). This shock front is expanding causing large azimuthal velocities and motions running around the star.

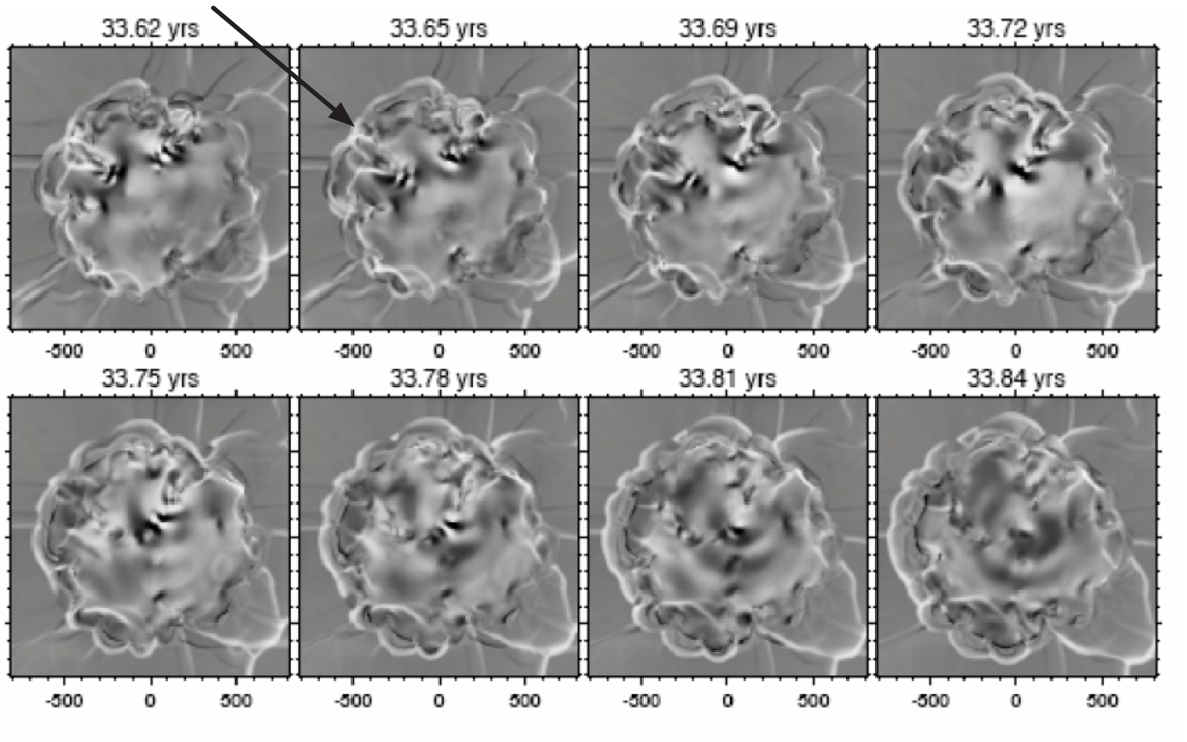

Figure 2.11: Sequence of temporal pressure fluctuations slices in a RHD model of red supergiant star. Every panel corresponds to the logarithmic difference in pressure between consecutive snapshots $5{\cdot}10^5$ s apart (to show rapid changes in pressure) multiplied by the temperature (to enhance fluctuations in the center). The x-axis is in solar radii. The black arrow indicates a shock wave hovering just above the stellar surface. Image courtesy of Bernd Freytag, 2008 in preparation.

2.3.4 Computational time

First, it must be said that the runs of temperature, opacity and heat capacity causes the local radiative relaxation time-scales to be much shorter than the hydrodynamical time-scale. Numerically, the radiative transport module needs to compute very short time steps and it is responsible of the relatively high computational cost of the simulations. Moreover, local fluctuations in opacity, temperature (i.e., affecting the source function), and heat capacity demands high stability of the radiation transport module.
The RSG models used in this work have been computed at:

- CINES (Centre Informatique National de l'Enseignement Supérieur) in Montpellier, on IBM Power4 computer nodes using 8 processors (CO^{5}BOLD is a parallel code)
- MacPro Intel, 4 processors with a clock speed of 3 GHz

Basically, running today a RSG simulations[9] would take about 100 days more or less continuously on both configurations reported above (perhaps 55 days on 16 processors).

[9]Starting it from a lower resolution model and not from scratch because this needs more time

However, due to the queueing system at CINES it would take about 1000 days, independent on the number of processors requested. The memory requirements is 2 GByte of RAM.
I report here also two important estimations of CPU time required for:

- non-grey simulations. The CPU time scales roughly with the number of bins: for 5 bins (non-grey) a single time-step would take about 5 times as long as a single bin (grey case). A possible solution could be to start with a long grey run and finish with a shorter non-grey run. In conclusion, the passage grey to non-grey (5 bins) treatment of opacity should require a factor 10 in CPU time even for a shorter run;

- higher resolution. The CPU time is proportional to resolution N^5, where N is the number of cells in each space direction, divided as follows: resolution N^3 due to the number of grid points and resolution N^2 due to the decreased time-step of the radiation transport.